NAA50 is an enzymatically active N-alpha-acetyltransferase that is crucial for development and regulation of stress responses

Laura Armbruster, Eric Linster, Jean-Baptiste Boyer, Annika Brünje, Jürgen Eirich, Iwona Stephan, Willy V. Bienvenut, Jonas Weidenhausen, Thierry Meinnel, Ruediger Hell, et al.

NAA50 Is an Enzymatically Active N^{α}-Acetyltransferase That Is Crucial for Development and Regulation of Stress Responses[1][OPEN]

Laura Armbruster,[a] Eric Linster,[a] Jean-Baptiste Boyer,[b] Annika Brünje,[c] Jürgen Eirich,[c] Iwona Stephan,[a] Willy V. Bienvenut,[b] Jonas Weidenhausen,[d] Thierry Meinnel,[b] Ruediger Hell,[a] Irmgard Sinning,[d] Iris Finkemeier,[c] Carmela Giglione,[b] and Markus Wirtz[a,2,3]

[a]Centre for Organismal Studies, Heidelberg University, 69120 Heidelberg, Germany
[b]Université Paris-Saclay, Commissariat à l'Energie Atomique, Centre National de la Recherche Scientifique, Institute for Integrative Biology of the Cell, 91198 Gif-sur-Yvette, France
[c]Institute for Plant Biology and Biotechnology, University of Münster, Muenster 48149, Germany
[d]Heidelberg University Biochemistry Center, 69120 Heidelberg, Germany

ORCID IDs: 0000-0002-4559-2404 (L.A.); 0000-0001-7963-1400 (E.L.); 0000-0001-5265-3917 (J.-B.B.); 0000-0002-8979-4606 (A.B.); 0000-0003-0963-1872 (J.E.); 0000-0003-4192-3920 (W.V.B.); 0000-0001-8376-2083 (J.W.); 0000-0001-5642-8637 (T.M.); 0000-0002-6238-4818 (R.H.); 0000-0001-9127-4477 (I.Si.); 0000-0002-8972-4026 (I.F.); 0000-0002-7475-1558 (C.G.); 0000-0001-7790-4022 (M.W.)

N^{α}-terminal acetylation (NTA) is a prevalent protein modification in eukaryotes. In plants, the biological function of NTA remains enigmatic. The dominant *N*-acetyltransferase (Nat) in Arabidopsis (*Arabidopsis thaliana*) is NatA, which cotranslationally catalyzes acetylation of ~40% of the proteome. The core NatA complex consists of the catalytic subunit NAA10 and the ribosome-anchoring subunit NAA15. In human (*Homo sapiens*), fruit fly (*Drosophila melanogaster*), and yeast (*Saccharomyces cerevisiae*), this core NatA complex interacts with NAA50 to form the NatE complex. While in metazoa, NAA50 has *N*-acetyltransferase activity, yeast NAA50 is catalytically inactive and positions NatA at the ribosome tunnel exit. Here, we report the identification and characterization of Arabidopsis NAA50 (AT5G11340). Consistent with its putative function as a cotranslationally acting Nat, AtNAA50-EYFP localized to the cytosol and the endoplasmic reticulum but also to the nuclei. We demonstrate that purified AtNAA50 displays N^{α}-terminal acetyltransferase and lysine-ε-autoacetyltransferase activity in vitro. Global *N*-acetylome profiling of *Escherichia coli* cells expressing AtNAA50 revealed conservation of NatE substrate specificity between plants and humans. Unlike the embryo-lethal phenotype caused by the absence of AtNAA10 and AtNAA15, loss of NAA50 expression resulted in severe growth retardation and infertility in two Arabidopsis transfer DNA insertion lines (*naa50-1* and *naa50-2*). The phenotype of *naa50-2* was rescued by the expression of HsNAA50 or AtNAA50. In contrast, the inactive ScNAA50 failed to complement *naa50-2*. Remarkably, loss of NAA50 expression did not affect NTA of known NatA substrates and caused the accumulation of proteins involved in stress responses. Overall, our results emphasize a relevant role of AtNAA50 in plant defense and development, which is independent of the essential NatA activity.

N^{α}-terminal acetylation (NTA) is a ubiquitous proteome-imprinting mechanism in eukaryotes. In humans and plants, 80% to 90% of cytosolic proteins are subject to NTA, which is catalyzed by N^{α}-acetyltransferases (Nats) that transfer an acetyl moiety from acetyl-CoA to the protein N terminus (Arnesen et al., 2009; Bienvenut et al., 2012; Drazic et al., 2016). Although NTA has been shown to affect the subcellular localization, aggregation, folding, and degradation of individual proteins, the overall significance of NTA is still unclear (Aksnes et al., 2016). In humans, seven Nat complexes (NatA to NatF and NatH) have been described. Each Nat complex is composed of at least one catalytic and facultative auxiliary subunits (Aksnes et al., 2015a, 2019). Whereas NatA to NatE (excluding NatD) are anchored to the ribosome via their auxiliary subunits and cotranslationally acetylate nascent polypeptide chains, NatF and NatH are monomeric and operate posttranslationally. Although putative orthologs for the catalytic subunits of NatA to NatF have been identified in plants by protein homology searches (Bienvenut et al., 2012; Breiman et al., 2016; Rathore et al., 2016), only NatA, NatB, and NatF have been biochemically characterized in plants so far (Ferrández-Ayela et al., 2013; Linster et al., 2015, 2020; Xu et al., 2015; Huber et al., 2020). Together, NatA and NatB target approximately three-fourths of extractable soluble proteins in Arabidopsis (*Arabidopsis thaliana*; Linster et al., 2015; Huber et al., 2020). The existence of a plant NatC has also been evidenced by functional complementation of a yeast NatC-deficient mutant, but the substrate specificity and subcellular localization of the plant NatC remain unexplored (Pesaresi et al., 2003). However, the ribosome association and substrate specificity of the core NatA and NatB are conserved between humans (*Homo sapiens*), yeast (*Saccharomyces cerevisiae*), and plants. The core NatA consists of the catalytic subunit NAA10 and the auxiliary subunit NAA15 and acetylates N termini starting with A, S, T, C, V, or G (Mullen et al., 1989;

Polevoda et al., 1999; Arnesen et al., 2009; Van Damme et al., 2011; Linster et al., 2015; Xu et al., 2015). The catalytic subunit NAA20 and the auxiliary subunit NAA25 form the NatB complex, which targets N termini retaining their initiator Met (iMet) followed by D, E, N, or Q (Polevoda et al., 1999; Van Damme et al., 2012; Huber et al., 2020). Although the biochemical features of the core NatA and NatB are evolutionarily conserved among eukaryotes, species-specific adaptations occurred in the remaining Nat machinery. Humans, for instance, possess a posttranslationally acting cytosolic NatH, which is not found in plants (Drazic et al., 2018). In contrast to metazoa, Arabidopsis possesses plant-specific organellar Nats that acetylates the N termini of plastid-encoded or imported proteins (Dinh et al., 2015; Bienvenut et al., 2020).

In humans and fruit fly (*Drosophila melanogaster*), the core NatA interacts with two additional proteins, HYPK and NAA50 (for review, see Aksnes et al., 2019). In both species, NAA50 binds to NatA to form the ternary NatE complex. NatE predominantly acetylates N termini starting with MS, MT, MA, MV, ML, MI, MF, MY, and MK (Evjenth et al., 2009; Van Damme et al., 2011; Gottlieb and Marmorstein, 2018; Aksnes et al., 2019). A putative ortholog of NAA50 has also been described in yeast and was shown to interact permanently with NatA in the ternary NatE complex associated with the ribosome (Gautschi et al., 2003; Knorr et al., 2019). Depletion of NAA50 impaired sister chromatid cohesion in human and fruit fly cells, resulting in mitotic arrest and segregation defects (Hou et al., 2007). This phenotype is absent in the yeast loss-of-NAA50 mutant, suggesting functional differences between NAA50 in yeast and metazoa. Different from human and fruit fly NAA50 homologs, yeast NAA50 lacks an optimal acetyl-CoA-binding motif and has recently been shown to be catalytically inactive (Deng et al., 2019). In agreement with this view, the knockout of NAA50 in yeast resulted in no decrease of NTA on canonical HsNAA50 substrates but caused a decrease in NTA of six NatA-type substrates. These findings suggest a regulatory impact of ScNAA50 on NatA activity in yeast (Van Damme et al., 2015). Structural analysis by cryoelectron microscopy demonstrates that ScNAA15 and ScNAA50 physically interact with rRNA expansion segments to position NAA10 at the ribosome tunnel exit. This exact positioning of NAA10 is supposed to facilitate the acetylation of the emerging polypeptide chain (Knorr et al., 2019).

Here, we identify and characterize Arabidopsis NAA50 (AT5G11340). We demonstrate that AtNAA50 is a catalytically active *N*-acetyltransferase of the NatE type with a substrate specificity similar to that of HsNAA50. In addition to its acetylation activity toward N^{α} termini, AtNAA50 can autoacetylate the ε-amino group of internal Lys residues (Kat activity) in vitro, as shown previously for the HsNAA50. The predominant localization of AtNAA50 in the nucleocytoplasma and at the endoplasmic reticulum (ER) is consistent with both its proposed function as a cotranslationally acting Nat and additional functions as a Kat. Loss of NAA50 in two Arabidopsis transfer DNA (T-DNA) insertion mutants (*naa50-1* and *naa50-2*) severely impairs vegetative plant growth and fertility but allows healthy embryo development. This phenotype is different from that of mutants lacking AtNAA10 and AtNAA15 function, whose development stops at the globular stage (Linster et al., 2015). The severe dwarfism of *naa50-2* can be complemented by the ectopic expression of catalytically active AtNAA50 or HsNAA50. In contrast, the catalytically inactive ScNAA50 failed to complement the growth phenotype of *naa50-2*. Finally, in *naa50-2*, the canonical NatA substrates were fully *N*-acetylated, but the absence of the acetylase induces the accumulation of many proteins involved in stress responses. In conclusion, our work suggests that AtNAA50 has more roles than merely being an auxiliary subunit of the NatA complex.

RESULTS

AtNAA50 Acts as a Nat with Broad Substrate Specificity

BLAST searches with NAA50 from human or yeast identify AT5G11340 as a putative ortholog of NAA50

[1]This work was supported by the Deutsche Forschungsgemeinschaft via the Collaborative Research Centre (grant no. SFP1036, TP13 to R.H. and M.W., TP 22 to I.Si., FI 1655/3–1 and INST 211/744–1 to I.F., and WI 3560/4–1 to M.W.) and by the Leibniz Programme (to I.Si). C.G. was supported by the Agence Nationale de la Recherche (grant no. ANR–10–LABX–0040–SPS) and by the facilities and expertise of the Institute of Integrative Biology of the Cell Service for the Identification and Characterization of Proteins by Mass Spectrometry proteomic platform, supported by Infrastructures in Biology Health and Agronomy, Ile de France Region, Plan Cancer, French National Centre for Scientific Research, and Paris-Sud University. R.H. and I.Si. are investigators of the Cluster of Excellence:CellNetworks. This project was carried out within the European Research Area Network for Coordinating Action in Plant Sciences Research Programme KatNat.

[2]Author for contact: markus.wirtz@cos.uni-heidelberg.de.

[3]Senior author.

The author responsible for distribution of materials integral to the findings presented in this article in accordance with the policy described in the Instructions for Authors (www.plantphysiol.org) is: Markus Wirtz (markus.wirtz@cos.uni-heidelberg.de).

I.St. identified and characterized the *naa50* mutants; L.A. performed the NAA50 subcellular localization studies and the in vitro acetylation assay; E.L. determined the Kat activity of NAA50 and the transcript levels of *NAA50*, *NAA10*, and *NAA15* in *naa50* mutants and wild-type plants; J.W. and I.Si. performed structure-function analyses of NAA50; C.G. and T.M. designed and supervised N-terminomics experiments; W.V.B. performed the GAP assay and profiled N termini of *naa50* mutants and wild-type plants; C.G., T.M., and J.-B.B. analyzed the N-terminomics data; I.St. and E.L. complemented the *naa50* mutants with endogenous, human, and yeast NAA50; A.B. and J.E. performed the quantitative proteome analysis of *naa50* mutants and wild-type plants; I.F. designed the proteome analysis experiment and supervised A.B. and J.E.; M.W. and R.H. conceived and directed the study; L.A. wrote the article with input from all authors.

[OPEN]Articles can be viewed without a subscription.

www.plantphysiol.org/cgi/doi/10.1104/pp.20.00222

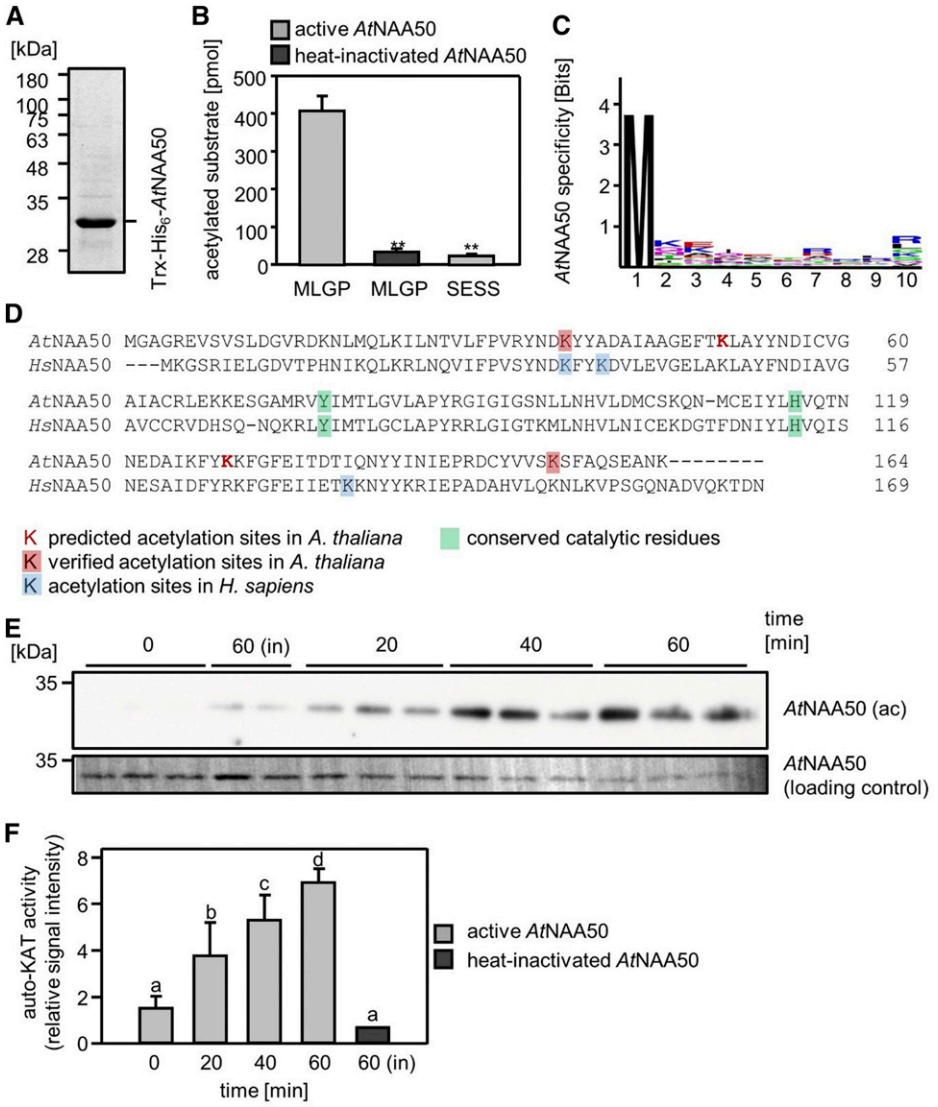

Figure 1. In vitro Nat and N^{ε}-Lys acetyltransferase (Kat) activity of AtNAA50. A, Trx-His_6-AtNAA50 was purified from *E. coli* by immobilized metal affinity chromatography. B, Purified Trx-His_6-AtNAA50 was incubated for 1 h at 37°C with 45 μM [^{3}H]acetyl-CoA and 0.2 mM of the synthetic MLGP and SESS peptides. After incubation, the peptide was enriched via specific interaction with SP Sepharose, and the amount of [^{3}H]acetyl incorporated in the peptide was quantified by scintillation counting. As a negative control, AtNAA50 was heat inactivated at 95°C for 10 min. Data are presented as means ± SD ($n = 4$, $P < 0.05$ by Student's *t* test). The experiment was repeated independently. C, Web logo of 28 N termini found to be specifically acetylated at their iMet after the expression of AtNAA50 in *E. coli*. D, Alignment of AtNAA50 and HsNAA50 protein sequences with Clustal Omega (https://www.ebi.ac.uk/Tools/msa/clustalo/). Lys residues that are acetylated in humans are shaded in blue; Lys residues that are acetylated in Arabidopsis are shaded in red. Lys residues that are predicted to be acetylated by Phosida (www.phosida.com) are marked in red. The conserved catalytic residues are shaded in green. E, Immunodetection of acetylated Lys residues on AtNAA50. Eleven micromolar purified AtNAA50 was incubated with 5 mM acetyl-CoA for 0, 20, 40, or 60 min at 37°C. Subsequently, the reaction was stopped by the addition of SDS loading buffer. The auto-Kat activity was determined via immunological detection of acetylated Lys residues with an α-acetylated Lys antibody. Heat-inactivated AtNAA50 (15 min at 95°C) served as a negative control (60 min). As loading control, AtNAA50 was visualized using Amido Black ($n = 3$). The experiment was repeated independently. F, Quantification of signals shown in E for the AtNAA50 autoacetylation. The Amido Black loading control was used for normalization. Data are presented as means ± SE. Different lowercase letters indicate individual groups identified by pairwise multiple comparisons with a Holm-Sidak one-way ANOVA ($P < 0.05$, $n = 3$).

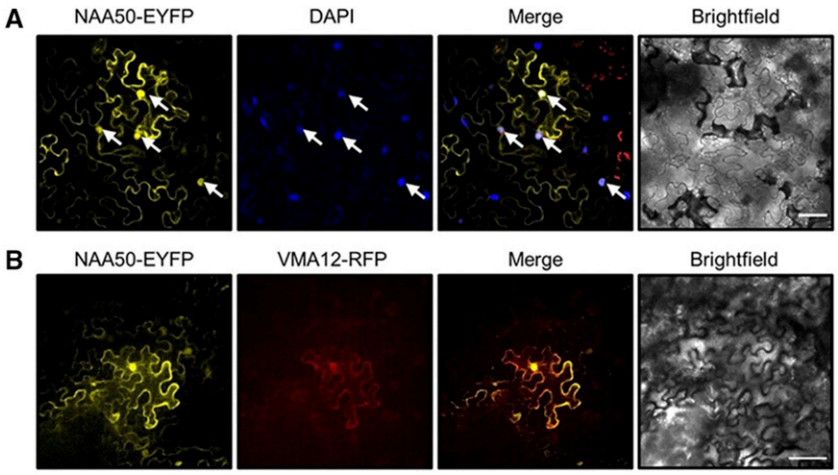

Figure 2. AtNAA50 is localized in the cytosol, the nucleus, and the ER. AtNAA50-EYFP was transiently expressed in *N. benthamiana* epidermal cells. A, Counterstaining with DAPI shows that AtNAA50-EYFP localizes to the nucleus (marked with arrows). B, AtNAA50-EYFP colocalizes with the RFP-tagged ER marker VMA12. The experiment was repeated independently. Bars = 50 μm.

in the Arabidopsis genome (Bienvenut et al., 2012; Neubauer and Innes, 2020). However, the enzymatic activity and substrate specificity of this putative plant NatE have not been characterized yet. Since HsNAA50 acetylates the NAA50 model substrate MLGP (Evjenth et al., 2009), we expressed Trx-His_6-AtNAA50 in *Escherichia coli* and subjected the purified enzyme (Fig. 1A) to an in vitro Nat activity assay with a custom-made MLGP peptide (Fig. 1B). Trx-His_6-AtNAA50 acetylated the MLGP peptide (specific activity $\geq$ 1.38 nmol min^{-1} mg^{-1}) but did not display Nat activity toward a canonical NatA substrate (SESS; Arnesen et al., 2009). This finding demonstrates that plant AtNAA50 is catalytically active toward substrates of the NatE type. To further elucidate the substrate specificity of plant NAA50, we heterologously expressed AtNAA50 in *E. coli* and performed a global acetylome profiling (GAP) assay. The analysis revealed 28 N termini to be specifically acetylated after the expression of AtNAA50 in *E. coli* (Supplemental Table S1). The vast majority of those N termini (25) were acetylated on their iMet. AtNAA50 was able to acetylate a wide range of N termini starting with the iMet, indicating a rather broad substrate specificity, with a weak preference for the polar amino acids Lys (K), Asn (N), Gln (Q), and Thr (T) at the second position (Fig. 1C).

HsNAA50 also displays Kat activity toward three internal Lys residues, K34, K37, and K140, in vitro (Evjenth et al., 2009). Similarly, three Lys acetylation sites (K37, K50, and K128) were predicted with high probability (greater than 0.9) in the plant NAA50 using Phosida (www.phosida.com; Fig. 1D). In recent Lys acetylome analyses of Arabidopsis, two Lys acetylation sites (K37 and K155) were experimentally determined (Hartl et al., 2017). To test for the autoacetylation of AtNAA50, the enzyme was incubated with acetyl-CoA for up to 60 min. Subsequently, acetylated Lys residues were visualized by immunological detection with an established commercially available α-acetylated Lys specific antibody (Fig. 1E). Acetylation of internal Lys residues increased linearly over the detection period and was absent when AtNAA50 was heat inactivated before incubation with acetyl-CoA (Fig. 1F).

NAA50 Localizes to the Nucleus, the Cytosol, and the ER

The subcellular localization of enzymes determines their access to substrates and potential interaction partners. Hence, after demonstrating the dual Kat/Nat activity of AtNAA50 in vitro, the subcellular localization of AtNAA50 was assessed in planta. For this purpose, an AtNAA50-enhanced yellow fluorescent protein (EYFP) fusion protein was transiently expressed in *Nicotiana benthamiana* epidermal cells that were either counterstained with the DNA-specific marker 4′,6-diaminophenylindole (DAPI; Fig. 2A) or cotransfected with the ER marker protein VMA12-RFP (Fig. 2B). In vivo live-cell imaging of the transfected leaves revealed that the AtNAA50-EYFP fusion protein displays a cytosolic pattern and colocalizes with both markers. To exclude that the nuclear localization of AtNAA50-EYFP was caused by overexpression of the fusion protein under the control of the 35S promoter, we expressed an AtNAA15-EYFP fusion protein in the same vector system. The resulting AtNAA15-EYFP fusion protein was not transported into the nucleus (Supplemental Fig. S1). These findings strongly suggest that AtNAA50 is localized in the nucleus, in the cytoplasm, and at the outer ER membrane. The cytoplasmic and ER-associated localization is in agreement with its putative function as a ribosome-associated Nat by interaction with AtNAA15.

NAA50 Is Critical for Plant Growth

In order to evaluate the biological function of NAA50 in plants, two homozygous T-DNA insertion lines (*naa50-1* [SAIL_1210_A02] and *naa50-2* [SAIL_1186_A03]) were identified (Supplemental Fig. S2). Sequencing of the genomic DNA from both lines revealed that a T-DNA was inserted in intron 1 of *NAA50* in *naa50-2* (position

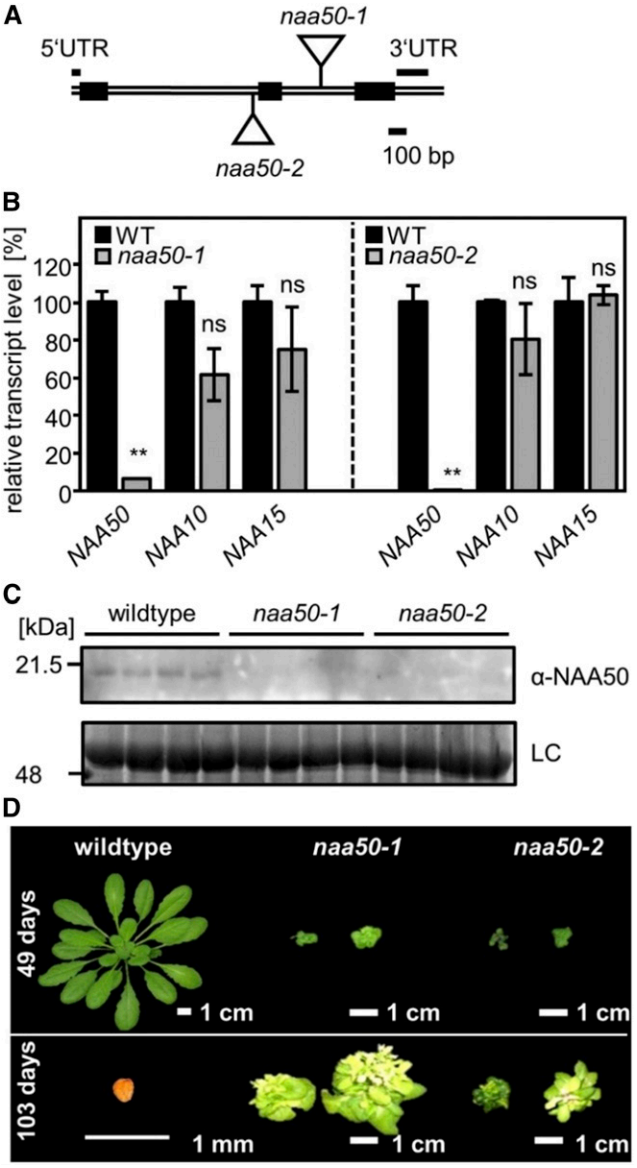

Figure 3. Mutations in NAA50 lead to a severe growth reduction and infertility. A, Gene model for AtNAA50 (AT5G11340). Black boxes represent exons. The two T-DNA insertion lines *naa50-1* (SAIL_1210_A02) and *naa50-2* (SAIL_1186_A03) are marked with triangles. UTR, Untranslated region. B, Transcript levels of *NAA50*, *NAA10*, and *NAA15* in *naa50-2* mutants and wild-type (WT) plants (Student's *t* test, $P < 0.05$, $n = 3$). The experiment was repeated independently. C, The NAA50 protein was detected with a specific antiserum in wild-type plants and *naa50-2* mutants. Amido Black staining of the transferred proteins on the membrane served as a loading control (LC). D, Representative images of homozygous *naa50-1* and *naa50-2* mutants compared with wild-type plants of the same age. Plants were grown for 8 weeks under short-day conditions and subsequently transferred to long-day conditions. Although occasionally *naa50* mutants were able to flower, none of these plants produced seeds. Images were digitally extracted for comparison.

1,159 bp after the start codon), while a T-DNA was integrated in the *NAA50* intron 2 at position 1,468 in the case of *naa50-1* (Fig. 3A). Reverse transcription quantitative PCR (RT-qPCR) for *NAA50* indicated the total absence of *NAA50* transcripts in both lines (Supplemental Fig. S3). Next, we characterized the impact of the T-DNA insertion in the *naa50-2* mutant on the transcription of *NAA50* and the core NatA subunits by RT-qPCR. RT-qPCR confirmed the absence of *NAA50* transcripts in *naa50-1* and *naa50-2*. However, the transcription of *NAA10* and *NAA15* remained unaffected (Fig. 3B), and also the protein levels of both NatA subunits were not significantly changed in *naa50-2* (see proteomic analysis, Supplemental Table S2). The latter findings were surprising since the down-regulation of one core NatA subunit by artificial microRNA interference caused cotranscriptional down-regulation of the other subunit, resulting in a decreased amount of both NatA core subunits (Linster et al., 2015). For that reason, we quantified the amount of NAA50 protein in the wild type and *naa50-2* with a specific antiserum. The NAA50 protein was readily detectable in the leaves of wild-type plants but was absent in *naa50* mutants (Fig. 3C). These findings demonstrate that *naa50-1* and *naa50-2* are real loss-of-NAA50 expression mutants, in which the transcriptional regulation and protein abundance of the core NatA subunits is unaffected.

Loss of the core NatA arrests embryo development at the globular stage (Linster et al., 2015). Both *naa50* lines finish embryo development and grow, apparently like the wild type, into the early seedling stage. However, after the formation of the first leaves, *naa50-1* and *naa50-2* show identical and severe retardation of growth. The vast majority of plants terminated growth after the development of a few small leaves. When grown in artificially high humidity under a transparent cover, very few mutants were able to flower, with a substantial delay in flowering time. None of these plants produced viable seeds (Fig. 3D). For that reason, homozygous plants from a segregating heterozygous *naa50-2* population were used for further experiments. Remarkably, the segregation pattern followed the expected 1:2:1 ratio, demonstrating that homozygous *naa50-2* pollen grows like the wild-type pollen, when they derive from a heterozygous *naa50-2* plant.

NAA50 Function Is Evolutionarily Conserved between Plants and Humans

Next, we wanted to provide direct evidence for the hypothesis that the severe growth retardation phenotype is caused by the absence of NAA50 activity. For that reason, the heterozygous *naa50-2* mutant was transformed with a construct expressing AtNAA50 under the control of the constitutive cauliflower mosaic virus (CaMV) 35S promoter ($_{Pro}$35-SCaMV:AtNAA50). The successful transformation was confirmed by selection on kanamycin, and complemented homozygous *naa50-2* were identified by PCR-based genotyping. The resulting complemented *naa50-2* mutants had a wild type-like habitus (Fig. 4A). Growth of *naa50-2*/$_{Pro}$35-SCaMV:AtNAA50, as determined by fresh weight production, was

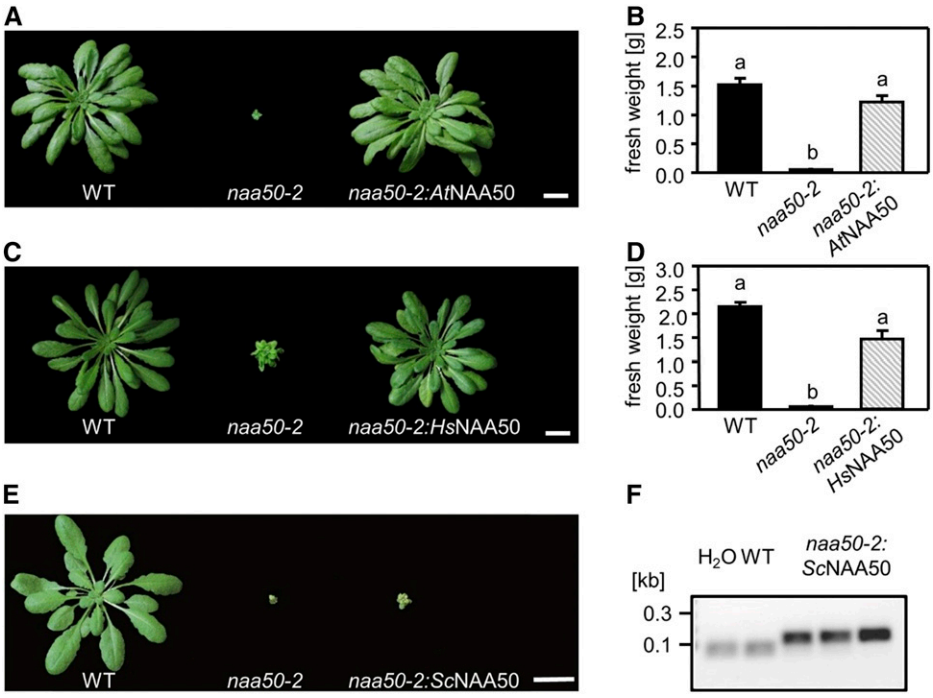

Figure 4. NAA50 function is conserved among humans and plants but not yeast. A, C, and E, Representative phenotypes of plants grown for approximately 8 weeks under short-day conditions. *naa50-2* mutants were complemented with AtNAA50 (A), HsNAA50 (C), and ScNAA50 (E). Images were digitally extracted for comparison. Bars = 2 cm. B and D, The fresh weight of *naa50-2* complemented with AtNAA50 (B) and HsNAA50 (D) was measured. The wild type (WT) served as a control. Data are presented as means ± SE. Statistically significant differences are indicated by different letters (Holm-Sidak one-way ANOVA, $P < 0.05$). This experiment was performed with $n > 5$ plants and was independently repeated. F, The expression of the ScNAA50 transcript in three individuals of *naa50-2*:ScNAA50 and the wild type was confirmed via RT-qPCR. A sample without genomic DNA (water) served as a negative control.

indistinguishable from the wild-type control (Fig. 4B). Remarkably, HsNAA50 was also able to rescue the Arabidopsis *naa50-2* slow-growth phenotype when expressed from the same construct (Fig. 4, C and D). In contrast, expression of the ScNAA50 protein failed to complement *naa50-2* (Fig. 4E), although transcription of ScNAA50 was confirmed by RT-qPCR in *naa50-2*/$_{Pro}$35-SCaMV:ScNAA50 (Fig. 4F). These findings strongly suggest that the evolutionarily conserved substrate specificities and enzymatic activities

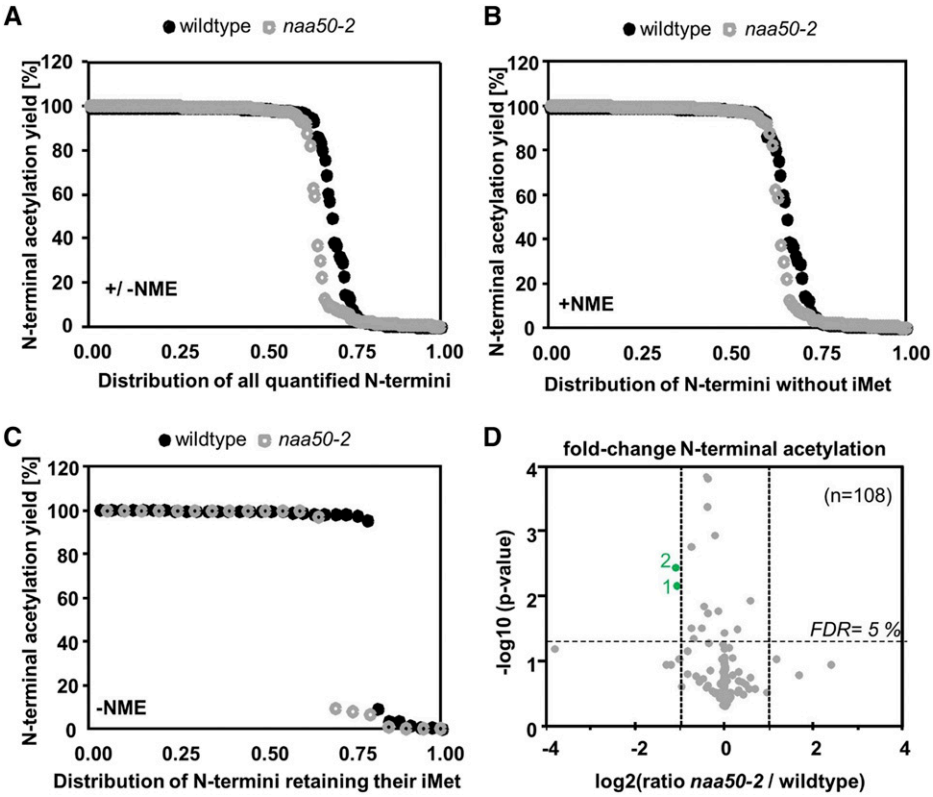

Figure 5. N-terminal protein acetylation in *NAA50*-depleted mutants. A to C, Distribution of the NTA yields in *naa50-2* (gray) and the wild type (black) for all quantified N termini (+/−N-terminal Met excision [NME]; A), N termini after removal of their iMet (+NME; B), and N termini retaining their iMet (−NME; C). D, Volcano plot of acetylated N termini found in the wild type and *naa50-2*. Proteins with statistically significant alteration of N-terminal acetylation yield are labeled in green ($P < 0.05$, greater than 2-fold change): 1, AT2G14880; 2, AT5G03370. For these experiments, whole plants were collected and pooled to obtain 100 mg of plant material of wild-type ($n = 2$) and *naa50-2* ($n = 3$) plants. FDR, False discovery rate.

Table 1. *The N-terminal acetylation yield of NatA substrates is unaffected in* naa50-2 *mutants*

Data are from proteins quantified in at least two biological replicate of the wild type and *amiNaa10*. When no quantitative acetylation data were obtained in the *naa50-2* data set, the N-terminal status was specified instead. In the cases of proteins 4 and 5, no significant quantification could be performed in *naa50-2* (dashes), but both N termini were identified as naturally acetylated (NTA), which indicates full acetylation.

Accession ARAPORT-11	Localization	NTA Position	N Terminus	Percentage NTA Ratio (*amiNaa10*:Wild Type)	Percentage NTA Ratio (*naa50-2*:Wild Type)
AT5G11670	Cytosol	2	GSTP	41.6	107.3
AT5G46790	Nucleus	2	ANSE	46.0	100.8
AT1G65930	Cytosol	2	AFEK	52.3	100.2
AT3G04920	Cytosol	2	AEKA	57.9	–
AT3G20050	Cytosol	2	SISA	58.8	–
AT3G23810	Cytosol	2	ALLV	59.8	100.3
AT3G53870	Cytosol	2	TTQI	69.1	100.1
AT2G36530	Cytosol	2	ATIT	78.3	100.0
AT3G52230	Plastid	2	AEEA	78.6	100.1

of AtNAA50 and HsNAA50 are required for the complementation of *naa50-2*.

Loss of NAA50 Does Not Affect NatA Activity in Plants

HsNAA50, DmNAA50, and ScNAA50 physically interact with the core NatA. Since ScNAA50 is supposed to act as a critical regulatory constituent of the NatA complex (Van Damme et al., 2015; Deng et al., 2020), we aimed to address the potential regulatory impact of AtNAA50 on NatA activity. To this end, we extracted soluble proteins from wild-type and *naa50-2* seedlings and determined their N-terminal acetylation status with the previously established stable isotope labeling protein N-terminal acetylation quantification (SILProNAQ) method (Bienvenut et al., 2017a). Analysis of the two genotypes identified 2,288 unique N termini corresponding to 1,043 nonredundant proteoforms and 824 distinct protein entities (PRIDE repository, identifier PXD017430). Among all identified proteoforms, 480 unique N termini (392 in the wild type and 309 in *naa50-2*) were quantified. Of the quantified N termini, 192 underwent the removal of iMet (40%) and 43 (9%) retained their iMet, while the remaining 245 (51%) are neo-N termini formed after intracellular maturation

Table 2. *List of the 20 most affected proteins by loss of NAA50*

Proteins were extracted from 4-week-old *naa50-2* mutants and wild-type plants grown on one-half-strength Murashige and Skoog (MS) plates under short-day conditions. This list only shows the 20 most prominently misregulated proteins in *naa50-2*. A full list of all quantified proteins can be found in Supplemental Table S2.

Protein Identifier	N Terminus	Description	Fold Change	*P*
AT2G43570	MAKPT	Chitinase	24.98	1.07E−07
AT2G18660	MIKMA	Encodes PNP-A (Plant Natriuretic Peptide A)	16.02	2.49E−06
AT3G57260	MSESR	β-1,3-Glucanase	15.30	3.30E−05
AT5G03350	MKIHK	Belongs to the group of early salicylic acid-activated genes	14.18	9.66E−06
AT5G37380	MECNK	Chaperone DnaJ-domain superfamily protein	13.20	1.58E−04
AT4G18253	MAKRL	Receptor Ser/Thr kinase-like protein	10.14	1.53E−03
AT1G02930	MAGIK	Encodes glutathione transferase belonging to the ϕ class of GSTs	9.80	1.31E−04
AT3G50930	MEGSK	Plays a role in cell death and amplifying salicylic acid signaling	8.69	9.05E−05
AT4G23600	MATLK	Encodes cystine lyase, which is expected to be involved in amino acid metabolism	8.68	5.97E−05
AT1G75040	MANIS	Thaumatin-like protein involved in response to pathogens	8.21	1.17E−04
AT3G28860	MSETN	Encodes a member of the ATP-binding cassette transporter family that is involved in auxin transport	0.23	2.48E−05
AT3G16450	MAQKV	Man-binding lectin superfamily protein	0.22	9.31E−06
AT3G16240	MAGVA	Δ-Tonoplast intrinsic protein, functions as a water channel and ammonium (NH_3) transporter	0.21	1.76E−04
AT3G01190	MAASK	Peroxidase superfamily protein	0.20	2.76E−05
AT4G28940	MGHFL	Phosphorylase superfamily protein	0.19	1.84E−04
AT5G54370	MEISK	Late embryogenesis abundant protein-like protein	0.16	5.91E−04
AT1G70850	MAKTE	MLP-like protein34	0.16	1.41E−06
AT2G01520	MATSG	Encodes a cis-cinnamic acid-responsive gene that is a member of the major latex protein-like gene family	0.14	1.42E−06
AT5G57560	MAITY	Encodes a cell wall-modifying enzyme, rapidly up-regulated in response to environmental stimuli	0.14	2.54E−03
AT5G15180	MAALK	Peroxidase superfamily protein	0.13	2.28E−03

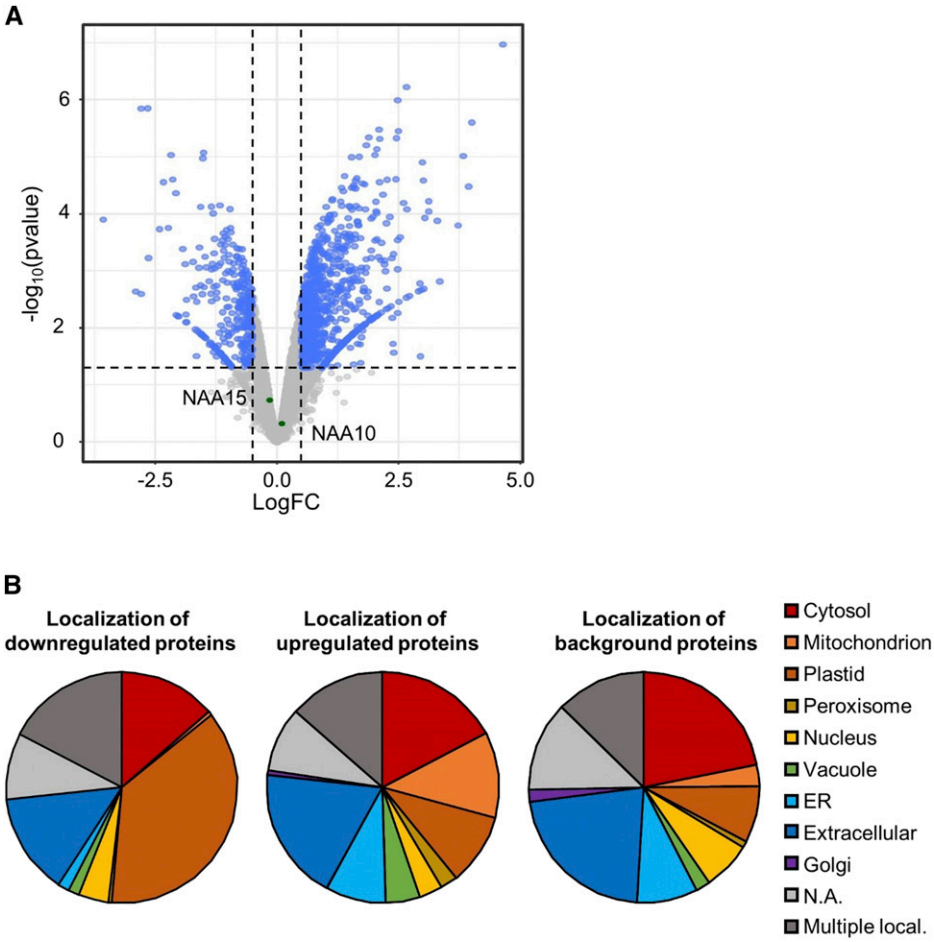

Figure 6. The expression of 732 protein groups is deregulated in *naa50-2* mutants compared with wild-type plants. A, Volcano plot depicting the significantly regulated (greater than 1.4-fold change, LIMMA $P < 0.05$, $n = 4$) protein groups in blue. Proteins with unaltered abundance in *naa50-2* are labeled in gray. NAA10 and NAA15 are indicated in green. Proteins were extracted from 4-week-old *naa50-2* and wild-type seedlings grown under short-day conditions on one-half strength MS medium. B, The differentially regulated proteins (first pie chart, down-regulated in *naa50-2* compared with the wild type; second pie chart, up-regulated in *naa50-2* compared with the wild type) are localized in a variety of cellular compartments, according to the SUBAcon localization of the SUBA4 Arabidopsis subcellular localization database (Hooper et al., 2017). For comparison, the distribution of localizations was calculated for all proteins detected in the MS approach (third pie chart, designated background). The full list of quantified protein groups is available in Supplemental Table S2. N.A., Not available.

(i.e. plastid-imported proteins). Here, we show that in the wild type, 66% (259 of 392) of the total quantified N termini were fully acetylated (acetylation yield > 95%), whereas 34% (133 of 392) were partially or not acetylated. Similarly, in the *naa50-2* mutant, 70% (215 of 309) of the total quantified N termini were fully acetylated and 30% (94 of 309) were partially acetylated, revealing no significant changes in terms of global NTA yield between the mutant and the wild type (Fig. 5A). Based on the GAP assay (Fig. 1C), AtNAA50 is expected to acetylate proteins retaining their iMet, whereas the NatA complex acts on proteins after removal of the iMet (Linster and Wirtz, 2018). Hence, we analyzed both populations separately (Fig. 5, B and C). When only N termini retaining their iMet (Fig. 5B) are considered, 26 N termini (79%, 26 of 33) are fully acetylated in wild-type plants compared with 13 N termini (65%, 13 of 20) retrieved in the mutants, revealing no significant difference between the two genotypes and therefore not providing any straightforward candidates for in vivo substrates of AtNAA50.

The same is true for N termini without iMet (Fig. 5C), where 99 N termini (60%, 99 of 166) are fully acetylated in wild-type plants compared with 74 N termini (59%, 74 of 126) in *naa50-2*, indicating that upon depletion of NAA50, NatA-type N termini remain acetylated. Indeed, previously identified NatA substrates, which are fully (greater than 95%) acetylated in wild-type plants and lose their acetylation marks upon knockdown of NAA10, retain their N-terminal acetylation levels in the *naa50-2* background (Table 1).

Of 108 N termini that were quantified in both the wild type and *naa50-2*, only two plastid proteins (AT2G1488 and AT5G03370) were found to be differentially acetylated (fold change > 2, $P < 0.05$; Fig. 5D). In both cases, the acetylation rates in the wild type were already low (1.9% for AT2G1488 and 13.9% for AT5G03370) and dropped to even lower levels in *naa50-2* (0.9% for AT2G1488 and 6.4% for AT5G03370).

Loss of NAA50 Causes the Accumulation of Stress Response Proteins

Although we could not identify any in vivo NAA50 substrates with the SILProNAQ approach, the severe phenotype of the *naa50* mutants suggested a vital role of AtNAA50 for the determination of proteome fate. A global comparison of the *naa50-2* mutant and the wild-type proteome revealed differential expression (greater than 1.4-fold up- or down-regulated, $P < 0.05$) of 732 protein

Table 3. *NAA50 mutants accumulate proteins involved in stress responses*

Proteins were extracted from 4-week-old *naa50-2* and wild-type seedlings grown under short-day conditions on one-half strength MS medium. Differentially regulated proteins (greater than 1.4-fold up- or down-regulated compared with the wild type; $P < 0.05$) were subjected to a Gene Ontology enrichment analysis performed with the DAVID Bioinformatics Resources tool v.6.8 (http://david.abcc.ncifcrf.gov). Proteins involved in the depicted biological processes were significantly (greater than 2-fold, $P < 0.05$) enriched upon the up- and down-regulated proteins. Counts represent the number of regulated proteins. For clarity, only stress-related biological processes are listed here; a full list of all affected biological processes is available in Supplemental Table S3.

Biological Process	Count	*P*	Fold Enrichment	False Discovery Rate
Up-regulated genes are involved in				
Systemic acquired resistance	14	7.4E−07	4.73	1.3E−03
Response to salicylic acid	15	9.0E−06	3.76	1.5E−02
Response to ER stress	10	9.3E−04	3.53	1.6E+00
Aerobic respiration	18	2.6E−05	3.04	4.3E−02
Response to ethylene	12	1.4E−03	2.92	2.4E+00
Programmed cell death	17	1.0E−04	2.87	1.8E−01
Defense response to fungus	27	3.2E−06	2.62	5.4E−03
Immune response	39	1.6E−08	2.59	2.7E−05
Response to jasmonic acid	13	2.6E−03	2.59	4.3E+00
Response to fungus	36	8.4E−08	2.57	1.4E−04
Cell death	20	1.3E−04	2.55	2.2E−01
Innate immune response	37	6.8E−08	2.55	1.2E−04
Immune system process	39	5.7E−08	2.49	9.7E−05
Response to wounding	19	3.3E−04	2.46	5.6E−01
Response to other organism	90	1.9E−15	2.29	3.2E−12
Response to biotic stimulus	92	1.7E−15	2.26	3.0E−12
Defense response	89	5.6E−13	2.11	9.5E−10
Response to bacterium	42	7.8E−06	2.02	1.3E−02
Down-regulated genes are involved in				
Cellular water homeostasis	10	2.9E−10	18.13	4.6E−07
Cell volume homeostasis	10	2.9E−10	18.13	4.6E−07
Water homeostasis	10	6.9E−10	16.92	1.1E−06
Regulation of cell size	12	2.8E−11	15.23	4.5E−08
Regulation of anatomical structure size	12	8.1E−08	8.23	1.3E−04
Cellular chemical homeostasis	12	1.1E−05	5.25	1.7E−02
Ion transmembrane transport	11	7.1E−04	3.63	1.1E+00
Chemical homeostasis	13	3.3E−04	3.40	5.3E−01
Cellular homeostasis	15	3.9E−04	2.97	6.2E−01
Cofactor biosynthetic process	13	2.6E−03	2.70	4.1E+00
Ion transport	15	1.8E−03	2.55	2.8E+00
Response to abiotic stimulus	50	2.1E−06	1.91	3.3E−03

groups, which corresponds to 16% of the quantified protein groups (4,508 protein groups; Supplemental Table S2). The 20 most affected proteins are listed in Table 2. The abundance of 541 protein groups increased significantly in *naa50-2*, while 191 protein groups were found to be down-regulated (Fig. 6A). The subcellular localization of these up-regulated proteins was diverse (Fig. 6B). Remarkably, 19% (compared with only 8% of all identified proteins) were localized in the extracellular space. The down-regulated proteins localize predominantly in the plastids (37%), the cytosol (14%), and the extracellular space (14%). The widespread subcellular distribution of the affected proteins suggests that the loss of AtNAA50 causes the observed alterations pleiotropically by disturbing relevant biological processes. To identify biological processes associated with NAA50, we performed a Gene Ontology enrichment analysis of the differentially regulated proteins using the DAVID Bioinformatics Resources tool v.6.8 (Table 3; Supplemental Table S3). The pathway enrichment analysis shows that proteins up-regulated in *naa50-2* are involved in a variety of stress responses, including immune system processes (2.5-fold enriched, $P < 0.05$) and the responses to the stress-related phytohormones salicylic acid (4-fold enriched, $P < 0.05$), jasmonic acid (3-fold enriched, $P < 0.05$), and ethylene (3-fold enriched, $P < 0.05$). Among the down-regulated proteins, proteins regulating cell size (15-fold enriched, $P < 0.05$), cell volume (18-fold enriched, $P < 0.05$), and ion transport (~3-fold enriched, $P < 0.05$) were overrepresented.

DISCUSSION

NAA50 Activity Is Functionally Conserved between Humans and Plants

NTA is the most abundant cotranslationally occurring protein modification in humans and Arabidopsis. The essential NatA complex targets approximately 40% of the proteome in both species, defining this complex

as one of the few globally acting protein modifiers in eukaryotic cells. In all eukaryotes analyzed so far (human, fruit fly, and yeast), NatA interacts with the NAA50 protein to form NatE, which gives rise to an independent NatE activity in humans and fruit flies. In contrast, ScNAA50 is enzymatically inactive (Deng et al., 2019). While enzymatic activity and the protein-protein interaction network of NAA50 have been extensively characterized in metazoa and fungi (Gautschi et al., 2003; Williams et al., 2003; Arnesen et al., 2005; Evjenth et al., 2009; Van Damme et al., 2011), the putative ortholog in plants was not characterized so far. Our work demonstrates that NAA50 is catalytically active in the reference plant Arabidopsis. AtNAA50 has a broad substrate specificity, which substantially overlaps with the substrate specificity of HsNAA50 (Van Damme et al., 2011; Reddi et al., 2016). Although we detect a preference of AtNAA50 for iMet followed by Lys (K), Asn (N), Gln (Q), and Thr (T) in the second position (Fig. 1C), expression of HsNAA50 is able to complement the loss of AtNAA50 in *naa50-2*. Complementation with the catalytically inactive ScNAA50 failed (Fig. 4C), suggesting that NAA50 activity is required to rescue *naa50-2*. Remarkably, catalytic residues are conserved in protein sequences of putative NAA50s in algae and plants (Supplemental Fig. S4), suggesting that NAA50 is catalytically active in phototrophic eukaryotes.

NatA Activity Is Not Modulated by NAA50

Although we demonstrate that AtNAA50 is catalytically active, the *N*-acetylome profiling approach did not allow us to identify any in vivo substrates that could explain the strong phenotype observed in the *naa50-2* mutant (Fig. 5D). This does not come as a surprise, since AtNAA50 is supposed to target only a few substrates (Ribeiro et al., 2016). While the combined activities of NatA and NatB target more than 75% of the extractable leaf proteome, NAA30, NAA50, and NAA60 together are thought to acetylate only 4% of the leaf proteome (Linster and Wirtz, 2018). For this reason, we cannot expect to identify a NatE substrate by the *N*-acetylome profiling approach, although it is state of the art. Despite the considerable overlap between the in vitro substrate specificities of AtNAA50 and AtNAA60, the enzymes may target distinct substrate pools due to their diverging subcellular localization in vivo. This spatial separation of substrate pools has also been suggested to occur in humans, where NAA60 mainly acetylates transmembrane proteins (Aksnes et al., 2015b; Van Damme et al., 2015).

Even though AtNAA50 displays catalytic activity on its own, the enzyme might have additional functions in association with the core NatA complex (Deng et al., 2020). This core complex is conserved between humans, yeast, and plants and consists of the catalytic subunit NAA10 and the auxiliary subunit NAA15 (Linster et al., 2015). In humans and yeast, the core complex interacts with the accessory subunit NAA50 (Gautschi et al., 2003; Van Damme et al., 2015). Until now, it was unclear whether NAA50 associates with the core NatA complex in plants. However, the colocalization of NAA10 and NAA50 was evidenced in the cytoplasm (Neubauer and Innes, 2020). Although ScNAA50 is inactive, it positively impacts NatA activity by modulating the enzymatic activity of ScNAA10 (Deng et al., 2019) and by positioning the NatA complex in close proximity to the ribosomal tunnel exit (Knorr et al., 2019). The interaction of NAA50 with the NatA complex is mediated via hydrophobic interactions between the NAA50 β2-β3 and β4-α2 loops and the NAA15 α22-α23 loop. A mutation in a highly conserved Thr residue in NAA15 (T416 in yeast and T406 in human) results in the dissociation of NAA15 from NAA50 in both yeast and human (Deng et al., 2019). This Thr residue (T412) is also conserved in Arabidopsis NAA15, suggesting a common NAA50-NAA15 binding mode. The N-terminome profiling approach, however, shows that the depletion of AtNAA50 does not result in decreased acetylation of NatA-type N termini (Table 1), revealing that, unlike ScNAA50, plant NAA50 is not required for the proper function of the NatA complex. Recently, the cryoelectron microscopy structure of the quaternary human NatE/HypK complex was reported and the authors show that HsNAA50 inhibits HsNatA activity in vitro (Deng et al., 2020). In plants, however, the absence of NAA50 does not induce any alteration of NTA on canonical NatA substrates under nonstressed conditions. We cannot exclude the possibility of stress-induced modifications of NatA/E subunits, which might alter their enzymatic activity or protein-protein interaction capability in plants, resulting in a more pronounced impact of NAA50 on NatA. One such modification might be Lys acetylation of NAA50, which has already been reported for the residues K37 and K155 (Hartl et al., 2017). The K37 residue is an evolutionarily conserved Lys acetylation site in humans and plants and is autoacetylated by HsNAA50 in vitro (Evjenth et al., 2009). Other modifications of the plant NatA/E subunits are currently unknown.

Depletion of NAA50 Leads to a Severe Growth Retardation

A possible explanation for the inhibited growth of *naa50* mutants is the constitutive induction of stress-related genes. We find that among the proteins accumulating in *naa50-2* mutants, proteins involved in the ER stress response are 3.4-fold overrepresented. The accumulation of ER stress-associated proteins can be explained by an enhanced transcription of these genes due to increased splicing of the transcription factor bZIP60 observed in *naa50-1* seedlings (Neubauer and Innes, 2020). Unspliced bZIP60 resides in the ER membrane due to a C-terminal transmembrane domain. In response to ER stress, bZIP60 is spliced by IRE1, which eliminates this C-terminal transmembrane domain, resulting in the translocation of bZIP60 into the nucleus, where it induces the expression of ER stress-responsive genes (Nagashima et al., 2011). In line with

this finding, proteins involved in the response to salicylic acid accumulate in *naa50-2* (3.7-fold). Salicylic acid is a primary regulator of plant growth particularly under stress conditions. During ER stress, salicylic acid diverts energy from plant growth to the induction of the unfolded protein response, thereby protecting the plant from misfolded proteins (Meng et al., 2017). Salicylic acid is also an important positive regulator of the plant immune response. In agreement with this finding, an increase in the expression of defense genes and salicylic acid signaling is observed in *naa50* mutants (Neubauer and Innes, 2020). We find this transcriptional increase reflected at the protein level (2.1-fold up-regulation of proteins involved in the defense response).

Since we show that AtNAA50-EYFP resides not only at the ER but also in the nucleus (Fig. 4, A and B), we cannot exclude a role of nucleus-localized NAA50 in the constitutive induction of stress responses in *naa50* mutants. The multiple localization of AtNAA50-EYFP in the cytosol and the ER has been independently confirmed by Neubauer and Innes (2020). The authors want to put a note of caution on the nuclear localization of AtNAA50-EYFP, since EYFP on its own is known to display nucleocytoplasmic localization (Chen et al., 2020). Hence, we cannot exclude that EYFP contributes to the nucleocytoplasmic localization of AtNAA50-EYFP. However, a nuclear localization of AtNAA50 is in agreement with both the nucleocytoplasmic localization of HsNAA50 (Arnesen et al., 2006) and a predicted bipartite nuclear localization signal at position 125 of AtNAA50 (Kosugi et al., 2009). In other species, acetyltransferases have already been shown to act as transcriptional regulators. HsNAA10 for instance regulates the response to hypoxia by ε-Lys acetylation of the transcription factor HIF-1α (Kang et al., 2018). Other studies report on the import of NAA10 into the nuclei of proliferating cells, where it is required for cell cycle progression and cell proliferation (Park et al., 2014). Such a scenario might also be conceivable for NAA50, suggesting that NAA50 is not always present in the nucleus. This would explain the apparent difference in the subcellular localization shown in our study and the results reported in Neubauer and Innes (2020).

CONCLUSION

In summary, we show that the catalytically active *N*-acetyltransferase AtNAA50 is required for plant growth and fertility. We demonstrate that its absence causes a severe growth reduction and an increase in diverse stress responses. Under optimal growth conditions, the acetylation of canonical NatA substrates was not affected by the loss of NAA50, demonstrating that NAA50 is dispensable for NatA activity in this condition. Our complementation studies point toward a conserved function of enzymatically active NAA50 in multicellular eukaryotes that is different from the function of inactive NAA50 in the unicellular budding yeast.

MATERIALS AND METHODS

Plant Material and Growth Conditions

This work refers to the Arabidopsis (*Arabidopsis thaliana*) ecotype Columbia-0 as the wild type. The T-DNA insertion lines *naa50-1* (SAIL_1210_A02) and *naa50-2* (SAIL_1186_A03) were obtained from the SAIL collection (Sessions et al., 2002). If not specified otherwise, experiments were conducted with plants grown on medium containing one-half soil and one-half substrate 2 (Klasmann-Deilmann) under short-day conditions (8.5 h of light, 100 μE light photon flux density, 24°C/18°C day/night temperatures, and 50% humidity). For growth on plates, seeds were surface sterilized with 70% (v/v) ethanol (5 min) and 6% (v/v) NaClO (2 min) followed by three washing steps with sterile water. After 2 d of stratification at 4°C, seeds were germinated on AT medium [5 mM KNO_3, 2.5 mM KH_2PO_4, pH 5.6, 2 mM $MgSO_4$, 2 mM $Ca(NO_3)_2$, 0.05 mM Fe-EDTA, 0.01 μM $CoCl_2$, 0.02 μM Na_2MoO_4, 0.5 μM $CuSO_4$, 1 μM $ZnSO_4$, 10 μM NaCl, 14 μM $MnCl_2$, and 0.8% [w/v] micro agar, pH 5.8].

Identification of the Putative *NAA50* Orthologs

The putative NAA50 homolog in Arabidopsis (AT5G11340) was identified as the result of a BLAST search (TAIR BLASTP2.2.8, www.arabidopsis.org) based on the *Saccharomyces cerevisiae* protein Naa50p (Yor253wp). AT5G11340 displayed a homology higher than any of the other putative homologs (score 61, E-value 3E-10). Similarly, homologs of AtNAA50 were identified in other organisms via a BLAST search (https://blast.ncbi.nlm.nih.gov/Blast.cgi?PAGE=Proteins) in *Homo sapiens* (UniProt ID: Q9GZZ1; 54% identity), *Oryza sativa* (UniProt ID: A2WSI1; 76% identity), *Glycine max* (UniProt ID: C6SYN6; 79% identity), *Chlamydomonas reinhardtii* (UniProt ID A8I4R4; 48% identity), *Vitis vinifera* (UniProt ID: A5BJF0; 81% identity), and *Populus trichocarpa* (UniProt ID: B9H9R5; 79% identity).

Extraction of Genomic DNA

In order to genotype the *naa50* mutants, genomic DNA was extracted from 50 to 100 mg of fresh Arabidopsis leaf material using Edwards buffer (200 mM Tris-HCl, 25 mM EDTA, 250 mM NaCl, and 0.5% [w/v] SDS). The tissue was ground in 400 μL of Edwards buffer using a plastic pestle. After vigorous mixing and centrifugation (5 min at room temperature), the supernatant was transferred to a fresh reaction tube and mixed with an equal amount of isopropanol. Subsequently, the samples were centrifuged at full speed for 10 min to allow nucleic acid precipitation. The supernatant was discarded and the pellet was washed with 70% (v/v) ethanol. After decanting the ethanol, the pellet was dried and resolved in 30 μL of sterile water.

PCR

Homozygous *naa50* mutants were identified by PCR-based genotyping using the FastGene Taq 2x Ready Mix (Nippon Genetics) and specific primer combinations for the wild-type (NAA50_fwd and NAA50_rev) and mutant (*naa50-1*, SAIL_LB and NAA50_rev; *naa50-2*, SAIL_LB and SAIL_RP) alleles.

For cloning, DNA was amplified with the high-fidelity DNA polymerase Phusion (New England Biolabs, M0530L). All enzymes were used according to the supplier's instruction manual. The corresponding primer sequences are listed in Supplemental Table S4.

Constructs for Complementation and Subcellular Localization in Plants

To analyze the conservation between putative NAA50 orthologs, the Arabidopsis *naa50-2* line was transformed with the endogenous NAA50 sequence as well as the human and yeast NAA50 sequences. The genes of interest were amplified from human, yeast, and plant cDNA via PCR using Gateway-compatible primers (AtNAA15-N, AtNAA15-C, AtNAA50-N, AtNAA50_STOP-C, HsNAA50-N, HsNAA50-C, ScNAA50-N, and ScNAA50-C). The protein sequences were then cloned into the binary vector pK2GW7.0, where they were expressed under the control of the CaMV 35S promoter. For localization, AtNAA50 was PCR amplified with the AtNAA50_N and AtNAA50_C primers and cloned via Gateway technology (Invitrogen) in the binary vector pB7YWG2.0, which contains the coding sequence for EYFP.

Stable Transformation of Arabidopsis

Stable transformation was conducted according to the floral dip method for *Agrobacterium tumefaciens*-mediated transformation of Arabidopsis described by Clough and Bent (1998). Transformants were selected on solidified medium [5 mM KNO_3, 2.5 mM KH_2PO_4, pH 5.6, 2 mM $MgSO_4$, 2.5 μM $Ca(NO_3)_2$, 50 μM Fe-EDTA, 70 μM H_3BO_3, 14 μM $MgCl_2$, 10 μM NaCl, 1 μM $ZnSO_4$, 0.5 μM $CuSO_4$, 0.02 μM Na_2MoO_4, 0.01 μM $CoCl_2$, and 0.8% micro agar, pH 5.8] supplemented with 50 μg mL^{-1} kanamycin.

Transient Transformation of *Nicotiana benthamiana* and Fluorescence Microscopy

The NAA50-EYFP fusion protein was expressed in *N. benthamiana* epidermal cells 24 to 48 h after *A. tumefaciens*-mediated transformation as described by Sparkes et al. (2006) with the pB7YWG2.0 construct. Leaves were either cotransfected with the ER marker VMA12-RFP (Viotti et al., 2013) or 2 μg μL^{-1} DAPI (Sigma-Aldrich). The fluorescence was analyzed by confocal laser scanning microscopy using a Nikon automated Ti inverted microscope equipped with a Yokagawa CSU-X1 confocal scanning unit, a Hamamatsu C9100-02 EMCCD camera, and a Nikon S Fluor 40× numerical aperture 1.3 oil-immersion objective (Nikon). Images were taken in three channels (RFP, 561/615; DAPI, 405/445 nm; and EYFP, 488/527 nm). Additionally, a bright-field image was recorded. The resulting images were processed with the open-source image-analysis software Fiji.

Constructs for Expression in *Escherichia coli* Cells

For the expression of AtNAA50 in *E. coli*, the NAA50 sequence was amplified from Arabidopsis cDNA with the primers NAA50_*Nco*I_fwd and NAA50_*Bam*HI_rev. Harnessing the newly established restriction sites, the resulting PCR fragment was cloned into the empty pETM20 or pETG10a vector (Dümmler et al., 2005).

Expression and Purification of AtNAA50 in *E. coli*

E. coli Rosetta (DE3; Novagen) was transformed by heat shock with the pETM2-AtNAA50 or pETG10a-AtNAA50 plasmid encoding for the Trx-His_6-AtNAA50 or His_6-AtNAA50 fusion protein. The expression of these recombinant proteins was induced with isopropyl-β-D-thiogalactoside (1 mM). After 5 h of incubation at 37°C, the cultures were harvested by centrifugation (10 min, 6,000*g*, 4°C). The pellet was dissolved in lysis buffer (250 mM NaCl, 20 mM imidazole, 0.5 mM phenylmethylsulfonyl fluoride, and 50 mM Tris, pH 8), and the cells were lysed by sonication. Trx-His_6-AtNAA50 was purified from the cell extracts by metal affinity chromatography on a HiTrap IMAC High-Performance column (GE Healthcare). For this purpose, the cell lysate was circulated on the column for 1 h. Afterward, the column was washed with wash buffer (250 mM NaCl, 80 mM imidazole, and 50 mM Tris, pH 8) and the protein was eluted in elution buffer (250 mM NaCl, 400 mM imidazole, and 50 mM Tris, pH 8). The quality of the purified protein was assessed by SDS-PAGE. The purified protein was used for in vitro acetyltransferase assays (Trx-His_6-AtNAA50; see below) and immunization of rabbits (His_6-AtNAA50) to generate an NAA50-specific antibody.

Generation of an AtNAA50-Specific Antiserum in Rabbit

For the immunization of the rabbits (treatments at days 0 and 30), 300 μL of purified His_6-AtNAA60 (~1 mg) was sterile filtered and mixed with 300 μL of Freund's complete adjuvant (Sigma-Aldrich). For the first and second boosts, the antigen was mixed with Freund's incomplete adjuvant (Sigma-Aldrich). The antibody titer was monitored 1 month after each injection via immunological detection by comparing the preimmune sera with the antibody-containing sera of the first and second antigen treatments (Supplemental Fig. S5). The immunization of the rabbits was stopped after the second boost. The blood samples were taken at day 44 and were stored for 24 h at 4°C followed by 20 min of centrifugation at ~30,000*g* and 4°C for 20 min. The resulting supernatant was supplemented with 0.2% (w/v) sodium azide and stored at −80°C until usage.

In Vitro NAT Assay

To measure the NAT activity of AtNAA50, 4.5 μg (150 pmol) of purified enzyme was mixed with 0.2 mM of a custom-made peptide (GeneCust), 0.2% (w/v) BSA in acetylation buffer (50 mM Tris-HCl, pH 7.5, 8 mM EDTA, and 1 mM DTT), and 45 μM [^{3}H]acetyl-CoA (7.4 GBq $mmol^{-1}$; tritium labeled only at the acetyl group by Hartmann Analytics). The reaction mix was topped up to 0.1 mL with acetylation buffer and incubated at 37°C for 1 h. Subsequently, the samples were centrifuged at 1,500*g* for 4 min. To isolate the custom-made peptide, the supernatant was mixed with 0.1 mL of SP Sepharose (50% [w/v] in 0.5 M acetic acid) and incubated for 5 min while shaking. After 4 min of centrifugation at 1,500*g*, the pellet was washed three times with 0.4 mL of 0.5 M acetic acid and once with 0.4 mL of 100% methanol. The amount of incorporated ^{3}H label was measured with a Tri-Carb 2810TR scintillation counter (Perkin-Elmer). The custom-made peptides MLGP (MLGPEGGRWGRPVGRRRRPVR-VYP) and SESS (SESSSRSRWGRPVGRRRRPVRVYP) share a C-terminal Arg-rich sequence resembling the human adrenocorticotropic hormone to facilitate peptide solubility and effective enrichment via Sepharose beads according to Evjenth et al. (2009).

In Vitro Kat Assay

To determine the Kat activity of AtNAA50, 11.5 μg (385 pmol) of purified enzyme was mixed with 1.92 μmol of acetyl-CoA in Kat buffer (50 mM Tris, 10% [v/v] glycerol, and 1 mM EDTA, pH 8.5) and incubated at 37°C. After 0 to 60 min, the reaction was stopped by adding 5 μL of 5× SDS loading buffer (0.1 M Tris, pH 7, 5% [w/v] SDS, 3.63 M β-mercaptoethanol, 20% [v/v] glycerol, and 0.01% [w/v] bromophenol blue) and subsequent incubation at 95°C for 10 min. The Kat activity was determined via immunological detection of acetylated Lys residues with an α-acetylated Lys antibody (1:10,000 in Tris-buffered saline plus Tween 20 with 5% [w/v] BSA, incubation overnight at 4°C; Cell Signaling, 9441).

Protein Extraction from Arabidopsis Leaf Tissue

Total soluble protein extracts were isolated from 200 mg of frozen and ground leaf material with 400 μL of precooled extraction buffer (50 mM HEPES, pH 7.4, 10 mM KCl, 1 mM EDTA, 11 mM EGTA, and 10% [v/v] glycerol) supplemented with 10 mM DTT and 0.5 mM phenylmethylsulfonyl fluoride. Protein extracts were cleared by centrifugation (10 min, 20,200*g*, 4°C), and the protein concentration was quantified according to Bradford (1976).

SDS-PAGE and Immunological Detection

Protein extracts were analyzed via SDS-PAGE (Laemmli, 1970) and blotted onto polyvinylidene difluoride membranes using Mini-Protean II cells (Bio-Rad). The primary NAA50 antibody and the secondary horseradish peroxidase-linked anti-rabbit antibody (no. AS10 852, Agrisera) were diluted 1:5,000 and 1:25,000 in 1× Tris-buffered saline plus Tween 20 (50 mM Tris, pH 7.6, 150 mM NaCl, and 0.05% [v/v] Tween 20) supplemented with 0.5% (w/v) BSA. Membranes were developed using the SuperSignal West Dura Extended Duration Substrate (Thermo Scientific) according to the manufacturer's instructions. The resulting signals were recorded using the ImageQuant LAS 4000 (GE Healthcare) and subsequently quantified with the ImageQuant TL software (GE Healthcare).

GAP and Data Analysis

GAP was performed as previously described by Dinh et al. (2015). For this purpose, 1 mg of *E. coli* lysates expressing AtNAA50-SUMO or SUMO-GFP as a negative control was subjected to chemical acetylation of free N termini with *N*-acetoxy-[2H3]-succinimide required for SILProNAQ quantification (Bienvenut et al., 2017a). The samples were digested with trypsin, and the N-terminal peptides were enriched by strong cation-exchange liquid chromatography before liquid chromatography-tandem mass spectrometry (LC-MS/MS) analysis. Raw data were extracted and exported with Proteome Discoverer (Thermo Scientific, version 1.4). The MASCOT 2.4 software was used for the identification of proteins and their cotranslational and posttranslational modifications. The *E. coli* K12 strain proteome extracted from UniProtKB (version 112) served as a reference proteome. The EnCOUNTer tool (Bienvenut et al., 2017b) was used to reprocess the quantified values determined by Mascot

Distiller and to supply a final list of the different peptides associated with their NTA yield.

N-Terminomics of Arabidopsis Wild-Type Plants and *naa50-2* Knockout Mutants

Arabidopsis wild-type and *naa50-2* mutant lines were grown for 4 weeks on one-half strength MS plates under short-day conditions. Whole plants were collected and pooled to obtain four replicates of 100 mg of plant material of wild-type and *naa50-2* plants. The plant tissue was frozen in liquid nitrogen and ground to a fine powder. Altogether, three biological replicates of *naa50-2* were used to characterize and quantify NTA following the protocol described in the above GAP test (Dinh et al., 2015).

LC-MS/MS-Based Quantitative Proteome Analyses

For the quantitative proteome analyses, plants were grown for 4 weeks on one-half strength MS plates under short-day conditions. Whole plants were collected and pooled to obtain four replicates of 100 mg of plant material of wild-type and *naa50-2* plants. The plant tissue was frozen in liquid nitrogen and ground to a fine powder. Protein extraction, sample processing, and LC-MS/MS data acquisition were performed as described previously (Lassowskat et al., 2017). Briefly, proteins were extracted and digested using a modified filter-assisted sample preparation protocol. Peptides were dimethyl labeled, whereby two replicates of each genotype were light labeled (dimethyl mass shift, +28.0313 D) and two replicates were medium labeled (dimethyl mass shift, +32.0564 D). Equal amounts of light-labeled and medium-labeled peptides were pooled for each replicate, desalted, and fractionated using SDB-RPS Stagetips (Kulak et al., 2014) followed by LC-MS/MS analyses. LC-MS/MS analyses were performed by using an EASY-nLC 1200 (Thermo Fisher) coupled to a Q Exactive HF mass spectrometer (Thermo Fisher). Separation of peptides was performed on 17-cm frit-less silica emitters (New Objective, 0.75 μm i.d.) and packed in-house with reverse-phase ReproSil-Pur C18 AQ 1.9 μm resin (Dr. Maisch). The column was constantly kept at 50°C. Peptides were eluted in 115 min applying a segmented linear gradient of 0% to 98% solvent B (solvent A, 0% acetonitrile and 0.1% [v/v] formamide; solvent B, 80% [v/v] acetonitrile and 0.1% [v/v] formamide) at a flow rate of 300 nL min^{-1}. Mass spectra were acquired in data-dependent acquisition mode according to the TOP15 method. MS spectra were collected by the Orbitrap analyzer with a mass range of 300 to 1,759 mass-to-charge ratio (*m/z*) at a resolution of 60,000 full width at half maximum, maximum injection time of 55 ms, and a target value of 3×10^6 ions. Precursors were selected with an isolation window of 1.3 *m/z*, and higher-energy collisional dissociation fragmentation was performed at a normalized collision energy of 25. MS/MS spectra were acquired with a target value of 105 ions at a resolution of 15,000 full width at half maximum, maximum injection time of 55 ms, and a fixed first mass of *m/z* 100. Peptides with a charge of +1, greater than 6, or with unassigned charge state were excluded from fragmentation for MS2, and the dynamic exclusion for 30 s prevented repeated selection of precursors.

Processing of raw data was performed using the MaxQuant software version 1.6.9.0 (Cox and Mann, 2008). MS/MS spectra were assigned to the Araport11 protein database. During the search, sequences of 248 common contaminant proteins as well as decoy sequences were automatically added. Trypsin specificity was required, and a maximum of two missed cleavages was allowed. Carbamidomethylation of Cys residues was set as a fixed modification, and oxidation of Met, deamidation, and protein N-terminal acetylation were set as variable modifications. Light and medium dimethylation of Lys residues and peptide N termini were set as labels. A false discovery rate of 1% for peptide spectrum matches and proteins was applied. Match between runs and requantify options were enabled. Further downstream analysis was performed using Perseus version 1.6.6.0 (Tyanova et al., 2016). Reverse hits and contaminants were removed, site ratios were $\log_2$ transformed, and flip-label ratios were inverted. Normalized site ratios were used for all further analyses. The resulting matrices were exported for the determination of significantly differential abundant protein groups using the LIMMA package (Ritchie et al., 2015) in R 3.3.1.

RT-qPCR

Nat transcript levels were analyzed by RT-qPCR as described previously (Huber et al., 2020). The corresponding primer sequences are listed in Supplemental Table S4.

Statistical Analyses

Statistical analysis was conducted using SigmaPlot 12.0. Means from different sets of data were analyzed for statistically significant differences with the Holm-Sidak one-way ANOVA test or Student's *t* test. Significant differences ($P < 0.05$) are indicated with different letters.

Accession Numbers

Sequence data from this article can be found in TAIR under Arabidopsis Genome Initiative accession numbers AT5G11340 (AtNAA50), AT3G06610 (AtHPYK) AT5G13780 (AtNAA10), and AT1G80410 (AtNAA15). The N-terminomics data are deposited at the PRIDE repository (https://www.ebi.ac.uk/pride/) with the data set identifier PXD017430. The full proteome data are deposited at the PRIDE repository (https://www.ebi.ac.uk/pride/) with the data set identifier PXD017663.

Supplemental Data

The following supplemental materials are available.

Supplemental Figure S1. NAA15-EYFP does not localize to the nucleus.

Supplemental Figure S2. Genotyping of homozygous *naa50* mutants.

Supplemental Figure S3. RT-qPCR reveals that the full-length NAA50 transcript cannot be detected in *naa50* mutants.

Supplemental Figure S4. Alignment of NAA50 from different phototrophic organisms.

Supplemental Figure S5. Validation of the specific antiserum against AtNAA50.

Supplemental Table S1. AtNAA50 GAP test.

Supplemental Table S2. Misregulated (greater than 2-fold up- or down-regulated; $P > 0.05$) proteins in *naa50-2* mutants compared with 4-week-old wild-type plants grown on one-half strength MS plates under short-day conditions.

Supplemental Table S3. Gene Ontology term enrichment analysis for differentially expressed proteins in NAA50-depleted plants.

Supplemental Table S4. Primers used for cloning, RT-qPCR, and genotyping.

ACKNOWLEDGMENTS

We thank Felix Alexander Weyer and Karine Lapouge (Heidelberg University Biochemistry Center) for fruitful discussions and careful reading and comments on the article.

Received February 24, 2020; accepted May 15, 2020; published May 27, 2020.

LITERATURE CITED

Aksnes H, Drazic A, Marie M, Arnesen T (2016) First things first: Vital protein marks by N-terminal acetyltransferases. Trends Biochem Sci **41:** 746–760

Aksnes H, Hole K, Arnesen T (2015a) Molecular, cellular, and physiological significance of N-terminal acetylation. Int Rev Cell Mol Biol **316:** 267–305

Aksnes H, Marie M, Arnesen T (2015b) Holding it together: Naa60 at the Golgi. Oncotarget **6:** 15726–15727

Aksnes H, Ree R, Arnesen T (2019) Co-translational, post-translational, and non-catalytic roles of N-terminal acetyltransferases. Mol Cell **73:** 1097–1114

Arnesen T, Anderson D, Baldersheim C, Lanotte M, Varhaug JE, Lillehaug JR (2005) Identification and characterization of the human ARD1-NATH protein acetyltransferase complex. Biochem J **386:** 433–443

Arnesen T, Anderson D, Torsvik J, Halseth HB, Varhaug JE, Lillehaug JR (2006) Cloning and characterization of hNAT5/hSAN: An evolutionarily conserved component of the NatA protein N-$^{\alpha}$-acetyltransferase complex. Gene **371:** 291–295

Arnesen T, Van Damme P, Polevoda B, Helsens K, Evjenth R, Colaert N, Varhaug JE, Vandekerckhove J, Lillehaug JR, Sherman F, et al (2009) Proteomics analyses reveal the evolutionary conservation and divergence of N-terminal acetyltransferases from yeast and humans. Proc Natl Acad Sci USA **106:** 8157–8162

Bienvenut WV, Brünje A, Boyer J-B, Mühlenbeck JS, Bernal G, Lassowskat I, Dian C, Linster E, Dinh TV, Koskela MM, et al (2020) Dual lysine and N-terminal acetyltransferases reveal the complexity underpinning protein acetylation. Mol Sys Biol **16:** e9464

Bienvenut WV, Giglione C, Meinnel T (2017a) SILProNAQ: A convenient approach for proteome-wide analysis of protein N-termini and N-terminal acetylation quantitation. In O Schilling, ed, Protein Terminal Profiling: Methods and Protocols. Springer, New York, pp 17–34

Bienvenut WV, Scarpelli JP, Dumestier J, Meinnel T, Giglione C (2017b) EnCOUNTer: A parsing tool to uncover the mature N-terminus of organelle-targeted proteins in complex samples. BMC Bioinformatics **18:** 182

Bienvenut WV, Sumpton D, Martinez A, Lilla S, Espagne C, Meinnel T, Giglione C (2012) Comparative large scale characterization of plant versus mammal proteins reveals similar and idiosyncratic N^{α}-acetylation features. Mol Cell Proteomics **11:** M111.015131

Bradford MM (1976) A rapid and sensitive method for the quantitation of microgram quantities of protein utilizing the principle of protein-dye binding. Anal Biochem **72:** 248–254

Breiman A, Fieulaine S, Meinnel T, Giglione C (2016) The intriguing realm of protein biogenesis: Facing the green co-translational protein maturation networks. Biochim Biophys Acta **1864:** 531–550

Chen J, Huang XY, Salt DE, Zhao FJ (2020) Mutation in *Os*CADT1 enhances cadmium tolerance and enriches selenium in rice grain. New Phytol **226:** 838–850

Clough S J, Bent A F (1998) Floral dip: A simplified method for *Agrobacterium*-mediated transformation of *Arabidopsis thaliana*. Plant J **16:** 735–743

Cox J, Mann M (2008) MaxQuant enables high peptide identification rates, individualized p.p.b.-range mass accuracies and proteome-wide protein quantification. Nat Biotechnol **26:** 1367–1372

Deng S, Magin RS, Wei X, Pan B, Petersson EJ, Marmorstein R (2019) Structure and mechanism of acetylation by the N-terminal dual enzyme NatA/Naa50 complex. Structure **27:** 1057–1070.e4

Deng S, McTiernan N, Wei X, Arnesen T, Marmorstein R (2020) Molecular basis for N-terminal acetylation by human NatE and its modulation by HYPK. Nat Commun **11:** 818

Dinh TV, Bienvenut WV, Linster E, Feldman-Salit A, Jung VA, Meinnel T, Hell R, Giglione C, Wirtz M (2015) Molecular identification and functional characterization of the first Nα-acetyltransferase in plastids by global acetylome profiling. Proteomics **15:** 2426–2435

Drazic A, Aksnes H, Marie M, Boczkowska M, Varland S, Timmerman E, Foyn H, Glomnes N, Rebowski G, Impens F, et al (2018) NAA80 is actin's N-terminal acetyltransferase and regulates cytoskeleton assembly and cell motility. Proc Natl Acad Sci USA **115:** 4399–4404

Drazic A, Myklebust LM, Ree R, Arnesen T (2016) The world of protein acetylation. Biochim Biophys Acta **1864:** 1372–1401

Dümmler A, Lawrence AM, de Marco A (2005) Simplified screening for the detection of soluble fusion constructs expressed in *E. coli* using a modular set of vectors. Microb Cell Fact **4:** 34

Evjenth R, Hole K, Karlsen OA, Ziegler M, Arnesen T, Lillehaug JR (2009) Human Naa50p (Nat5/San) displays both protein N^{α}- and N^{ε}-acetyltransferase activity. J Biol Chem **284:** 31122–31129

Ferrández-Ayela A, Micol-Ponce R, Sánchez-García AB, Alonso-Peral MM, Micol JL, Ponce MR (2013) Mutation of an Arabidopsis NatB N-$^{\alpha}$-terminal acetylation complex component causes pleiotropic developmental defects. PLoS ONE **8:** e80697

Gautschi M, Just S, Mun A, Ross S, Rücknagel P, Dubaquié Y, Ehrenhofer-Murray A, Rospert S (2003) The yeast N^{α}-acetyltransferase NatA is quantitatively anchored to the ribosome and interacts with nascent polypeptides. Mol Cell Biol **23:** 7403–7414

Gottlieb L, Marmorstein R (2018) Structure of human NatA and its regulation by the Huntingtin interacting protein HYPK. Structure **26:** 925–935.e928

Hartl M, Füßl M, Boersema PJ, Jost JO, Kramer K, Bakirbas A, Sindlinger J, Plöchinger M, Leister D, Uhrig G, et al (2017) Lysine acetylome profiling uncovers novel histone deacetylase substrate proteins in *Arabidopsis*. Mol Syst Biol **13:** 949

Hooper CM, Castleden IR, Tanz SK, Aryamanesh N, Millar AH (2017) SUBA4: The interactive data analysis centre for Arabidopsis subcellular protein locations. Nucleic Acids Res **45:** D1064–D1074

Hou F, Chu CW, Kong X, Yokomori K, Zou H (2007) The acetyltransferase activity of San stabilizes the mitotic cohesin at the centromeres in a shugoshin-independent manner. J Cell Biol **177:** 587–597

Huber M, Bienvenut WV, Linster E, Stephan I, Armbruster L, Sticht C, Layer D, Lapouge K, Meinnel T, Sinning I, et al (2020) NatB-mediated N-terminal acetylation affects growth and biotic stress responses. Plant Physiol **182:** 792–806

Kang J, Chun YS, Huh J, Park JW (2018) FIH permits NAA10 to catalyze the oxygen-dependent lysyl-acetylation of HIF-1α. Redox Biol **19:** 364–374

Knorr AG, Schmidt C, Tesina P, Berninghausen O, Becker T, Beatrix B, Beckmann R (2019) Ribosome-NatA architecture reveals that rRNA expansion segments coordinate N-terminal acetylation. Nat Struct Mol Biol **26:** 35–39

Kosugi S, Hasebe M, Tomita M, Yanagawa H (2009) Systematic identification of cell cycle-dependent yeast nucleocytoplasmic shuttling proteins by prediction of composite motifs. Proc Natl Acad Sci USA **106:** 10171–10176

Kulak NA, Pichler G, Paron I, Nagaraj N, Mann M (2014) Minimal, encapsulated proteomic-sample processing applied to copy-number estimation in eukaryotic cells. Nat Methods **11:** 319–324

Laemmli UK (1970) Cleavage of structural proteins during the assembly of the head of bacteriophage T4. Nature **227:** 680–685

Lassowskat I, Hartl M, Hosp F, Boersema PJ, Mann M, Finkemeier I (2017) Dimethyl-labeling-based quantification of the lysine acetylome and proteome of plants. Methods Mol Biol **1653:** 65–81

Linster E, Stephan I, Bienvenut WV, Maple-Grødem J, Myklebust LM, Huber M, Reichelt M, Sticht C, Møller SG, Meinnel T, et al (2015) Downregulation of N-terminal acetylation triggers ABA-mediated drought responses in Arabidopsis. Nat Commun **6:** 7640

Linster E, Wirtz M (2018) N-terminal acetylation: An essential protein modification emerges as an important regulator of stress responses. J Exp Bot **69:** 4555–4568

Linster E, Layer D, Bienvenut WV, Dinh TV, Weyer FA, Leemhuis W, Brünje A, Hoffrichter M, Miklankova P, Kopp J, et al (2020) The Arabidopsis N^{a}-acetyltransferase NAA60 locates to the plasma membrane and is vital for the high salt stress response. New Phtyol doi: 10.1111/nph.16747

Meng Z, Ruberti C, Gong Z, Brandizzi F (2017) CPR5 modulates salicylic acid and the unfolded protein response to manage tradeoffs between plant growth and stress responses. Plant J **89:** 486–501

Mullen JR, Kayne PS, Moerschell RP, Tsunasawa S, Gribskov M, Colavito-Shepanski M, Grunstein M, Sherman F, Sternglanz R (1989) Identification and characterization of genes and mutants for an N-terminal acetyltransferase from yeast. EMBO J **8:** 2067–2075

Nagashima Y, Mishiba K, Suzuki E, Shimada Y, Iwata Y, Koizumi N (2011) Arabidopsis IRE1 catalyses unconventional splicing of bZIP60 mRNA to produce the active transcription factor. Sci Rep **1:** 29

Neubauer M, Innes RW (2020) The Arabidopsis N-terminal acetyltransferase NAA50 regulates plant growth and defense. bioRxiv 893115

Park JH, Seo JH, Wee HJ, Vo TT, Lee EJ, Choi H, Cha JH, Ahn BJ, Shin MW, Bae SJ, et al (2014) Nuclear translocation of hARD1 contributes to proper cell cycle progression. PLoS ONE **9:** e105185

Pesaresi P, Gardner NA, Masiero S, Dietzmann A, Eichacker L, Wickner R, Salamini F, Leister D (2003) Cytoplasmic N-terminal protein acetylation is required for efficient photosynthesis in Arabidopsis. Plant Cell **15:** 1817–1832

Polevoda B, Norbeck J, Takakura H, Blomberg A, Sherman F (1999) Identification and specificities of N-terminal acetyltransferases from *Saccharomyces cerevisiae*. EMBO J **18:** 6155–6168

Rathore OS, Faustino A, Prudêncio P, Van Damme P, Cox CJ, Martinho RG (2016) Absence of N-terminal acetyltransferase diversification during evolution of eukaryotic organisms. Sci Rep **6:** 21304

Reddi R, Saddanapu V, Chinthapalli DK, Sankoju P, Sripadi P, Addlagatta A (2016) Human Naa50 protein displays broad substrate specificity for amino-terminal acetylation: Detailed structural and biochemical analysis using tetrapeptide library. J Biol Chem **291:** 20530–20538

Ribeiro AL, Silva RD, Foyn H, Tiago MN, Rathore OS, Arnesen T, Martinho RG (2016) Naa50/San-dependent N-terminal acetylation of Scc1 is potentially important for sister chromatid cohesion. Sci Rep **6:** 39118

Ritchie ME, Phipson B, Wu D, Hu Y, Law CW, Shi W, Smyth GK (2015) limma powers differential expression analyses for RNA-sequencing and microarray studies. Nucleic Acids Res **43:** e47

Sessions A, Burke E, Presting G, Aux G, McElver J, Patton D, Dietrich B, Ho P, Bacwaden J, Ko C, et al (2002) A high-throughput Arabidopsis reverse genetics system. Plant Cell **14:** 2985–2994

Sparkes IA, Runions J, Kearns A, Hawes C (2006) Rapid, transient expression of fluorescent fusion proteins in tobacco plants and generation of stably transformed plants. Nat Protoc **1:** 2019–2025

Tyanova S, Temu T, Sinitcyn P, Carlson A, Hein MY, Geiger T, Mann M, Cox J (2016) The Perseus computational platform for comprehensive analysis of (prote)omics data. Nat Methods **13:** 731–740

Van Damme P, Evjenth R, Foyn H, Demeyer K, De Bock PJ, Lillehaug JR, Vandekerckhove J, Arnesen T, Gevaert K (2011) Proteome-derived peptide libraries allow detailed analysis of the substrate specificities of N^{α}-acetyltransferases and point to hNaa10p as the post-translational actin N^{α}-acetyltransferase. Mol Cell Proteomics **10:** M110.004580

Van Damme P, Hole K, Gevaert K, Arnesen T (2015) N-terminal acetylome analysis reveals the specificity of Naa50 (Nat5) and suggests a kinetic competition between N-terminal acetyltransferases and methionine aminopeptidases. Proteomics **15:** 2436–2446

Van Damme P, Lasa M, Polevoda B, Gazquez C, Elosegui-Artola A, Kim DS, De Juan-Pardo E, Demeyer K, Hole K, Larrea E, et al (2012) N-terminal acetylome analyses and functional insights of the N-terminal acetyltransferase NatB. Proc Natl Acad Sci USA **109:** 12449–12454

Viotti C, Krüger F, Krebs M, Neubert C, Fink F, Lupanga U, Scheuring D, Boutté Y, Frescatada-Rosa M, Wolfenstetter S, et al (2013) The endoplasmic reticulum is the main membrane source for biogenesis of the lytic vacuole in Arabidopsis. Plant Cell **25:** 3434–3449

Williams BC, Garrett-Engele CM, Li Z, Williams EV, Rosenman ED, Goldberg ML (2003) Two putative acetyltransferases, san and deco, are required for establishing sister chromatid cohesion in Drosophila. Curr Biol **13:** 2025–2036

Xu F, Huang Y, Li L, Gannon P, Linster E, Huber M, Kapos P, Bienvenut W, Polevoda B, Meinnel T, et al (2015) Two N-terminal acetyltransferases antagonistically regulate the stability of a nod-like receptor in Arabidopsis. Plant Cell **27:** 1547–1562